

UNDERSTANDING PHOSPHORUS EMITTER DIFFUSION IN SILICON SOLAR CELL PROCESSING

A. Bentzen^{a)}, J.S. Christensen^{b)}, B.G. Svensson^{b)}, and A. Holt^{a)}

^{a)} Section for Renewable Energy, Institute for Energy Technology, P.O. Box 40, NO-2027 Kjeller, Norway.

^{b)} Department of Physics, Centre for Materials Science and Nanotechnology, University of Oslo, P.O. Box 1048 Blindern, NO-0316 Oslo, Norway

ABSTRACT: High concentration in-diffusion of phosphorus from a spray-on source is a promising method for in-line emitter diffusion in p-type silicon solar cell processing. Increasing the understanding of the physical mechanisms behind phosphorus diffusion in silicon is therefore of great importance in order to facilitate optimization of the diffusion process. In this paper, the main mechanisms responsible for dopant transport during phosphorus emitter diffusion in solar cell processing are identified and described, and an integrated diffusion model is presented for simulation of such emitter profiles. It is found that the occurrence of the kink-and-tail profile shape, characteristic of high concentration phosphorus diffused emitters, is caused by a changeover from a vacancy-mediated diffusion at high concentrations to an interstitially driven diffusion at lower concentrations. This changeover involves a transition via migration of self-interstitials, limiting diffusion in the so-called kink region to restore local point defect equilibrium. It is further found that the three distinct diffusion regimes all exhibit Arrhenius behaviors, thus a model for emitter diffusion involving only three free parameters, namely the diffusion temperature, the diffusion time, and the phosphorus surface concentration, can be employed to accurately simulate emitter diffusion profiles.

Keywords: Diffusion, Phosphorus, Modeling.

1 INTRODUCTION

Phosphorus (P) in-diffusion is currently the primary method for emitter fabrication in silicon (Si) solar cell processing. Although the physics of P diffusion in Si have been studied for more than 40 years, little comprehensive research have been reported on high concentration P in-diffusion relevant for especially multicrystalline Si (mc-Si) solar cell manufacturing.

The current Si feedstock shortage has, at least temporarily, shifted the focus of solar cell and mc-Si wafer manufacturers from ‘larger’ to ‘thinner’. High Si feedstock prices are similarly favoring “cut-free” wafer technologies having a lower Si consumption loss, such as string ribbons (STR) or edge defined film growth ribbons (EFG), typically being limited in the maximum sizes achievable. To minimize the cost consequence of the size handicap of smaller wafers in batch-type processing, in-line processes for solar cell manufacturing are obtaining a significant interest from the industry. Due to this, an increased attention to substituting the long-lasting standard of the batch POC₃ emitter diffusion to in-line diffusion from e.g. a spray-on process is to be expected.

Understanding the physical mechanisms behind P diffusion in Si is essential in order to optimize the emitter processing in solar cell manufacturing. In this work, P diffusion in Si is described, providing the basis for an integrated diffusion model to fully simulate high concentration P diffused emitter profiles obtained from an in-line process.

2 DIFFUSION IN SILICON

2.1 Dopant diffusion

On the macroscopic one-dimensional scale, diffusion of a foreign species in Si can under equilibrium conditions be described by Fick’s second law:

$$\frac{\partial}{\partial x} \left(D_A \frac{\partial C_A}{\partial x} \right) = \frac{\partial C_A}{\partial t}, \quad (1)$$

where C_A is the species concentration in the host material,

and D_A is the concentration dependent diffusivity of the species. Fickian diffusion, as empirically described by the above equation, requires that the material in which the specie diffuses is homogeneous (e.g. that the species solubility is spatially invariant), and that diffusion is promoted only by the thermodynamic force caused by a concentration gradient of the species. For a general consideration of P diffusion in Si, the first of these requirements is assumed to be valid.

When a charged dopant, such as P⁺, diffuses in Si, the force exerted on the dopants is no longer determined by the thermodynamics alone. Diffusion of an ionized dopant causes a spatially varying Fermi level, and thus an internal electric field will be present during diffusion. Moreover, it is known that dopant diffusion in Si prevails primarily by interaction with intrinsic point defects (i.e. vacancies and self-interstitials), the concentrations of which are dependent on the Fermi level position. Although dopants may also diffuse by directly exchanging lattice sites with an adjacent crystal atom, such concerted exchange diffusion is believed to be of minor importance for dopant diffusion in Si [1].

Considering diffusion of a donor A^+ interacting with intrinsic point defects X (a vacancy or an interstitial/interstitialcy) under the influence of both a thermodynamic and an electrostatic force, it can be shown through extensive elaboration that the *effective* dopant diffusivity in interaction with a specific intrinsic point defect X can be described as [2]

$$D_{A^+X^{-m}} = h D_{A^+X^{-m}}^i \left(\frac{n}{n_i} \right)^m, \quad (2)$$

where the superscript i indicates the dopant diffusivity under intrinsic point defect conditions, X^m denotes the point defect of charge state m that governs the diffusion, n is the electron concentration, and n_i is the intrinsic electron concentration at the diffusion temperature. The charge state m of the point defect is *defined* as a positive number for a negative charge state, thus a positively charged point defect results in a negative exponent in equation (2). In the above equation, h is referred to as the field enhancement factor defined as

$$h = 1 + \frac{C_{A^+}}{2n_i} \left[\left(\frac{C_{A^+}}{2n_i} \right)^2 + 1 \right]^{-1/2}, \quad (3)$$

acting to promote diffusion due to the spatially varying Fermi level.

2.2 Extracting the diffusivity

The diffusion equation (1) can generally not be solved analytically nor numerically to reveal the diffusivity when the latter is dependent on the concentration. However, by reverse analysis from experimentally measured diffusion profiles, the concentration dependent diffusivity can be extracted. One such procedure for reverse analysis is the Boltzmann-Matano method, the basis of which is defining a plane in the diffusion geometry, referred to as the Matano interface X_M , where the concentration of dopants remains constant during diffusion. It can then be shown (see e.g. [3]) that the diffusivity can be calculated from the diffusion profile $C_A(x)$ according to

$$D_A(C_A) = -\frac{1}{2t} \left(\frac{dx}{dC_A} \right)_{C_A} \int_{C_A}^{C'_A} (x - X_M) dC_A, \quad (4)$$

where C'_A is the dopant concentration at which the concentration gradient becomes zero, i.e. at sufficiently large depths into the sample.

The culprit of the Boltzmann-Matano analysis is the identification of the Matano interface. Upon in-diffusion from an external source, however, the appropriate choice for the Matano interface is $X_M = 0$ if the source can be regarded as infinite, i.e. under experimental conditions where the concentration at the surface is independent of the diffusion time.

3 EXPERIMENTAL DETAILS

In this work, P diffused emitters were prepared by in-diffusion from the spray-on source Filmtronics P509 on neighboring $10 \times 10 \text{ cm}^2$ boron (B) doped mc-Si wafers of $1 \text{ } \Omega\text{cm}$ nominal resistivity. Prior to application of the diffusion source, the wafers were treated in a 10% NaOH damage etch followed by an additional chemical polish consisting of $\text{HNO}_3:\text{HF}:\text{CH}_3\text{COOH}$ (10:2:5). The diffusion source was applied by pressurized air spraying, baked at 120°C to remove the solvents, and the samples were diffused in an IR-heated belt furnace at different temperatures and durations. Finally, the residual diffusion source was removed by etching in HF.

To measure the diffusion profiles, secondary ion mass spectrometry (SIMS) was performed using Cs^+ sputtering ions with a net energy of 13.5 keV. All measurements were conducted within equivalent grains of the different samples. The concentration dependent P diffusivity was consequently extracted from the measured diffusion profiles employing the Boltzmann-Matano method as briefly described above, providing the basis for modeling the diffusion process. As P diffused emitters suitable for screen-printed solar cells typically exhibit concentrations towards the surface exceeding the limit of electrically active P in Si, the electric profile deviates from the chemical profile as measured by SIMS [3,4]. Therefore, the profiles of electrically active P were

measured by electrochemical capacitance-voltage (ECV) profiling, similarly conducted within equivalent grains of the different samples.

4 RESULTS AND DISCUSSION

In Fig. 1, the P concentration profile as measured by SIMS after in-diffusion from the spray-on source at 890°C for 1218 seconds is shown (open circles). As is seen in the figure, the profile reveals the characteristic kink-and-tail shape, in which a faster diffusing tail prevails at low concentrations. Considering the concentration of electrically active dopants, we have previously shown that a close relation with the chemical profile exists for concentrations below $2\text{-}3 \times 10^{20} \text{ cm}^{-3}$, saturating at a practically constant level for concentrations exceeding this limit [3,4]. This saturation level is in good agreement with the limit of electrically active P in equilibrium with inactive dopants [5].

Employing the Boltzmann-Matano method according to equation (4) on the above diffusion profile provides the concentration dependent phosphorus diffusivity at the specific diffusion temperature, exhibited in Fig. 2 (open circles). In the current experiments, the Matano interface $X_M = 0$ has been introduced due to the observed invariant surface concentration with diffusion time [3].

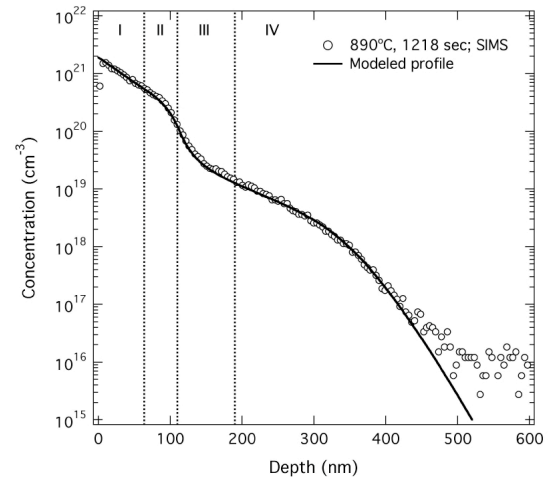


Figure 1: Phosphorus diffusion profile as measured by SIMS (open circles) and modeled (solid line) after in-diffusion at 890°C for 1218 seconds.

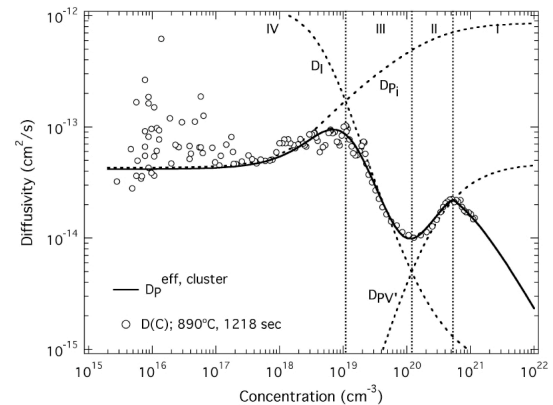


Figure 2: Phosphorus diffusivity as extracted by the Boltzmann-Matano analysis (open circles) and modeled (solid line) after in-diffusion at 890°C for 1218 seconds.

When P diffuses in Si, interaction with both self-interstitials and vacancies occur according to the diffusion reactions



and



where Si_{Si} denotes a substitutional Si atom, P_{Si} is a substitutional dopant, e is an electron, Si_i is a self-interstitial, and V is a vacancy. In equation (5), P_i denotes an interstitial (or an interstitially paired) dopant. In the following, diffusion of P by an interstitial mechanism will be denoted as P_i , although it is generally not possible to distinguish between diffusion of an interstitial dopant and a dopant-interstitial pair, the latter referring to a dopant in interaction with a long range configurational disorder involving ‘‘bonded’’ interstitials [6].

At low concentrations, it is generally known that P diffuses in Si primarily by interaction with self-interstitials [7], through kick-out reactions as described in equation (5). In a purely interstitial-substitutional diffusion mechanism, local point defect equilibrium must be restored by supply (or dissipation) of self-interstitials from (or to) the surface [8]. Therefore, low concentration diffusion is governed by both migration of interstitial P (or dopant-interstitial pairs) as well as diffusion of self-interstitials to restore local point defect equilibrium, and the overall dopant diffusivity at low concentrations is limited by the slower of these two processes [8,9]. The transition between these processes corresponds to the interface between regions IV and III in Fig. 2.

At higher concentrations, however, it has previously been shown that when the P concentration becomes sufficiently large, the population of doubly negative vacancies will increase significantly [2], and thus an onset of a vacancy-mediated diffusion described by equation (6) will occur. The critical P concentration for this onset is when the Fermi level reaches the energy position of the doubly negative vacancy charge state, i.e. at 0.11 eV below the conduction band edge. We have previously shown that this concentration corresponds to the interface between regions III and II in Fig. 2 [3].

When a dopant diffuses by a dual diffusion mechanism, i.e. in interaction with both self-interstitials and vacancies, the overall effective dopant diffusivity is the sum of the two individual mechanisms [10]. Hence, the effective P diffusivity can be expressed as [3,8,9]

$$D_P = \frac{D_{P_i} D_I}{D_{P_i} + D_I} + D_{PV''}, \quad (7)$$

where each of the individual diffusivities is described according to equation (2). This diffusivity model is included in Fig. 2 (solid line, below region I), and each of the individual diffusion mechanisms are shown as dashed lines in the figure. Adapting equations (7) and (2) to experimentally extracted diffusivity data from diffusions at different temperatures and durations, we have previously shown that each of the three different diffusion mechanisms are characterized by Arrhenius behaviors; $D^i = D_0 \exp(-E_d/k_B T)$ [3]. An overview of the thus extracted diffusion parameters is provided in Table I.

Table I: Overview of the diffusion parameters relevant to high concentration in-diffusion of P in Si.

	Region	D_0 (cm ² /s)	E_d (eV)	Exponent
D_{P_i}	IV	$(5.8 \pm 0.1) \times 10^{-5}$	2.1 ± 0.1	0.5
D_I	III	$(2.3 \pm 0.2) \times 10^{-1}$	2.6 ± 0.2	-1.8
$D_{PV''}$	II	$(7.6 \pm 0.4) \times 10^4$	5.2 ± 0.3	2

It should be noted that there is a slight deviation between the data in Table I and those presented in [3], due to a correction of the field enhancement factor at low concentrations used in [3]. Furthermore, utilization of the above diffusion model requires the knowledge of the electron density during diffusion. As briefly mentioned above, the concentration of electrically active dopants deviates from the chemical concentration at high doping levels. By comparing the chemical profiles as measured by SIMS with the electrically active profiles as measured by ECV, we have previously found that the following empirical relation can be applied [3]

$$C_P = C_{P^+} + \frac{2(1.6 \times 10^{-41}) C_{P^+}^3}{1 - (1.6 \times 10^{-41}) C_{P^+}^2}. \quad (8)$$

The electron concentration is further related to the concentration of electrically active dopants through the law of mass action under requirements of charge neutrality according to

$$n = \frac{1}{2} \left(C_{P^+} + \sqrt{C_{P^+}^2 + 4n_i^2} \right). \quad (9)$$

The diffusivity model according to equation (7) is, however, only capable of describing the P diffusivity at concentration below the interface between regions II and I, as seen in Fig. 2. A decreasing diffusivity as exhibited in region I has previously been argued to be due to cluster formation when the dopant concentration becomes sufficiently large [11,12]. Under the assumption that only the unclustered dopants are mobile, Solmi et al. [12] showed that the effective diffusivity could then be expressed as

$$D_{P,cluster} = D_P \left(\frac{C_{mob}}{C_P} \right), \quad (10)$$

where C_P and C_{mob} are the total and mobile P concentrations, respectively. Thus, the interface between regions II and I in Fig. 2 denotes the concentration at which P clustering occurs, believed to coincide with the solid solubility limit at the diffusion temperature.

In Fig. 3, the concentration at this interface is shown versus the reciprocal diffusion temperature (solid and open circles) as extracted after in-diffusion at different temperatures and durations. The dashed line in the figure corresponds to the solid solubility limit presented by Solmi et al. [5], whereas the solid line is an empirical fit to the present experimental data according to

$$C_{sat} = 4.1 \times 10^{22} \exp\left(\frac{-0.44 \text{ eV}}{k_B T}\right) \text{ cm}^{-3}. \quad (11)$$

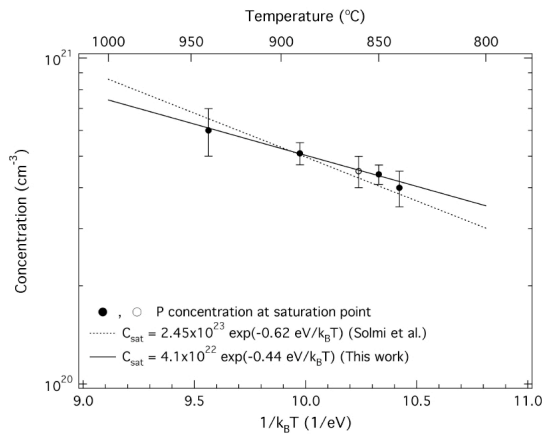


Figure 3: Phosphorus concentration at the saturation point (solid circles – in-line diffusion; open circle – POCl_3 diffusion), as well as an empirical fit (solid line) and the solid solubility limit (dashed line) as reported by Solmi et al. [5].

The concentration of mobile P atoms can thus be described as

$$C_{mob} = \begin{cases} C_{sat} & \text{if } C_P > C_{sat} \\ C_P & \text{otherwise} \end{cases}, \quad (12)$$

which together with equations (2), and (7) – (12) provides a comprehensive model to explain the P diffusion. This model is included in Fig. 2 as the solid line, and evidently provides close description of the concentration dependent diffusivity at all concentrations. Similarly, solving Fick's second law as described in equation (1) using the finite element numerical software FEMLAB [13] using the full diffusivity model including clustering, the solid line in Fig. 1 clearly shows that an accurate simulation of the P diffusion profile can be obtained. To achieve such simulations, only three free parameters are required; the diffusion temperature, the diffusion time, and the P concentration near the surface.

To summarize, P diffusion in Si can be divided in four separate regions as indicated in both Figs. 1 and 2. In region IV, corresponding to the tail of the profile, diffusion is governed by interaction with self-interstitials or interstitialcies, referred to as *I*-type diffusion. A transition occurs at the interface to region III, where migration of self-interstitials to restore local point defect equilibrium commences to limit the diffusion of P. In region III, corresponding to the kink region of the profile, this self-interstitial limited diffusion prevails. When the P concentration becomes sufficiently high to raise the Fermi level above 0.11 eV below the conduction band edge, as is the case at the interface between regions III and II, the large increase in doubly negative vacancies promotes a vacancy-mediated diffusion in region II. At the highest concentrations towards the surface, exceeding the solubility limit as indicated by the interface between regions II and I causes formation of clusters, leading to a P-rich layer near the surface in region I and a consequent decreasing diffusivity of the clustered atoms.

5 CONCLUSIONS

This work gives an overview of the mechanisms occurring during high concentration in-diffusion of

phosphorus in silicon, and thus serves as a step towards further understanding of emitter diffusion in silicon solar cell processing. It is shown that the characteristic kink-and-tail profile shapes arise due to a changeover from a vacancy-mediated diffusion at high concentrations to an interstitially driven diffusion at lower concentrations. In the transition between these two regimes, lowering of the Fermi level causes dissociation of the dopant-vacancy pairs, and migration of self-interstitials in order to restore local point defect equilibrium limits the diffusion of P. With such an increased understanding of the P diffusion mechanism, simulation and consequential optimization of the diffusion process for n^+ emitter formation is made possible.

ACKNOWLEDGMENTS

This work was financed in part by the Research Council of Norway. The authors are indebted to Dr. Margareta Linnarson at the Royal Institute of Technology (Sweden) for assistance with the SIMS measurements, as well as Dr. Radovan Kopecek at the University of Konstanz (Germany) for assisting with the ECV profiling.

REFERENCES

- [1] C.S. Nichols, C.G. Van de Walle, S.T. Pantelides, *Physical Review B* 40 (1989) 5484.
- [2] P.M. Fahey, P.B. Griffin, J.D. Plummer, *Reviews of Modern Physics* 61 (1989) 289.
- [3] A. Bentzen, J.S. Christensen, B.G. Svensson, A. Holt, *Journal of Applied Physics* 99 (2006) 064502.
- [4] A. Bentzen, A. Holt, *Proceedings 31st IEEE Photovoltaic Specialists Conference* (2005) 1153.
- [5] S. Solmi, A. Parisini, R. Angelucci, A. Armigliato, D. Nobili, L. Moro, *Physical Review B* 53 (1996) 7836.
- [6] G.D. Watkins, R.P. Messmer, C. Weigel, D. Peak, J.W. Corbett, *Physical Review Letters* 27 (1971) 1573.
- [7] A. Ural, P.B. Griffin, J.D. Plummer, *Journal of Applied Physics* 85 (1999) 6440.
- [8] S. Yu, T.Y. Tan, U. Gösele, *Journal of Applied Physics* 70 (1991) 4827.
- [9] M. Uematsu, *Journal of Applied Physics* 82 (1997) 2228.
- [10] D. Mathiot, J.C Pfister, *Journal of Applied Physics* 55 (1984) 3518.
- [11] R.B. Fair, G.R. Weber, *Journal of Applied Physics* 44 (1973) 273.
- [12] S. Solmi, D. Nobili, *Journal of Applied Physics* 83 (1998) 2484.